IEEE Access
Multidisciplinary | Rapid Review | Open Access Journal

Received September 11, 2020, accepted September 26, 2020, date of publication September 29, 2020,
date of current version October 12, 2020.

Digital Object Identifier 10.1109/ACCESS.2020.3027638

Gate-Error-Resilient Quantum Steane Codes

ROSIE CANE[1], DARYUS CHANDRA[2], SOON XIN NG[1], (Senior Member, IEEE), AND LAJOS HANZO[1], (Fellow, IEEE)

[1]School of Electronics and Computer Science, University of Southampton, Southampton SO17 1BJ, U.K.
[2]Department of Electrical Engineering and Information Technology, University of Naples Federico II, 80138 Naples, Italy

Corresponding author: Lajos Hanzo (lh@ecs.soton.ac.uk)

The work of Lajos Hanzo was supported in part by the Engineering and Physical Sciences Research Council (COALESCE) under Project EP/N004558/1, Project EP/P034284/1, Project EP/P034284/1, and Project EP/P003990/1; in part by the Royal Society's Global Challenges Research Fund Grant; and in part by the European Research Council's Advanced Fellow Grant QuantCom.

ABSTRACT An encoderless quantum code is capable of connecting quantum information by replacing the encoder circuit with a fault-tolerant single-qubit gate arrangement. As a further benefit, in contrast to state preparation techniques, our encoderless scheme requires no prior knowledge of the input information, therefore totally unknown states can be encoded fault-tolerantly. Our encoderless quantum code delivers a frame error rate that is three orders of magnitude lower than that of the corresponding scheme relying on a non-fault-tolerant encoder, when the gate error probability is as high as 10^{-3}.

INDEX TERMS Fault tolerance, quantum error correction codes, quantum stabilizer codes, quantum gates, Encoderless quantum code.

I. INTRODUCTION

A quantum error correction code (QECC) must be implemented by a fault-tolerant circuit that is capable of avoiding avalanche-like error-proliferation[1] in quantum gates. More explicitly, a fault-tolerant circuit limits the effects of a single gate error to a correctable number of qubit errors [1]. However, unfortunately many traditional encoding circuits are not fault-tolerant [1]–[3]. This is because these circuits have two-qubit controlled-NOT (CNOT) gate connections which have the property that a single qubit error propagates to many qubits, hence proliferating the errors [4]. This overwhelms the error correction capability of the $[n, k, d]$ QECC, hence more errors are inflicted by the circuit than are corrected, where n is the number of encoded physical qubits, k is the number of original information qubits, d is the minimum distance and t is the error correction capability where we have $t = (d-1)/2$ for the family of maximum-minimum distance codes. Therefore, rather than satisfying our original objective of improving the error rates, the QECC failing to rely on a fault-tolerant architecture prepares encoded states that have a higher error rate than the original uncoded information [3].

To mitigate these problems, we present an alternative scheme that prepares encoded quantum states without applying non-fault-tolerant encoding circuits. More explicitly, this outputs an encoded state with a Frame-Error-Rate[2] (FER) that is lower than that of the uncoded information, even when the gate error probability is high. This is achieved by using a circuit, which is entirely comprised only of single-qubit gates. Hence the resultant circuit has a fault-tolerant arrangement, in which no error proliferation can occur. Rather than directly encoding the information using a quantum error correction encoder, this '*encoderless*' scheme first prepares an n-qubit state that is a superposition of legitimate codewords or correctable error patterns. The resultant encoded state is carefully chosen so that any error patterns within the code's correction capability can be corrected by the syndrome decoder. As a benefit, following the action of the syndrome decoder, only valid codewords are created which represent the n-qubit encoded version of the k-qubit input information. Again we refer to our proposed method as the '*encoderless scheme*'.

This approach is reminiscent of quantum state preparation techniques [5]. Further investigations of Steane code state preparation were presented in [6]–[9], where the logical states such as $|\overline{0}\rangle$ and $|\overline{+}\rangle$ are prepared fault-tolerantly. Improvements that minimize the ancilla qubit overheads required for Steane code state preparation were provided in [10]. In addition, methods of preparing the encoded states of longer codes

The associate editor coordinating the review of this manuscript and approving it for publication was Zhen Ren.

[1]We define error-proliferation as the event when a single error inflicts more than one error. This is in contrast to error-propagation, which passes on the same number of errors as its input.

[2]A frame error event is defined as the occurrence of more than the number of correctable errors t

were conceived in [11] for circumventing the employment of complex encoding circuits. Finally, state preparation assuming a local 2D-architecture was designed in [12], [13].

The scheme presented here has the added benefit that it can be applied to unknown input information, implying that we have no prior knowledge of the state before encoding. In this paper, what is referred to as a *known* state $|\psi\rangle$ is one whereby we do have prior knowledge of the value of the complex probability amplitudes α and β in the state $|\psi\rangle = \alpha|0\rangle + \beta|1\rangle$. Therefore, with no knowledge about the value of α and β the state is said to be *unknown*.

Unitary encoding and decoding circuits are prone to the proliferation of errors, because the circuits are not fault tolerant and therefore they inflict more errors than the QECC can correct [2], [4], [5]. The scheme presented in this paper offers fault tolerant encoding of unknown states with the aid of a single stabilizer measurement and two extra Hadamard gates. The ability to encode states with no prior knowledge of the information qubits will be necessary for systems relying on multiple networked devices. Another benefit of this scheme is that it has a simpler circuit than the state preparation schemes for certain known states [6]. This is advantageous in near-intermediate-scale-quantum (NISQ) processors having limited qubit coherence times and error-infested circuit components [14]. However, the prerequisite for using this scheme is that it needs clean all-zero ancilla qubits in order to achieve fault-tolerance. In addition, this scheme relies on a full stabilizer measurement, which is costly compared to the non-fault tolerant unitary encoding circuit in terms of qubit overheads [3], [15]. Nevertheless, if the architectural assumptions of the stabilizer circuit are met by the processor, the encoderless scheme imposes no further connectivity constraints on the device. Therefore the implementation is likely to be applicable to a number of state-of-the art devices, where the stabilizer measurements can be readily implemented.

Based on the aforementioned background, our novel contributions are:

1) *We propose a technique of preparing the n-qubit encoded version of a k-qubit quantum state using imperfect quantum logic gates that are prone to the deleterious effects of decoherence both to repetition codes and to Steanes code. This scheme has the added benefit that it does not require prior knowledge of the information to be encoded. We demonstrate that provided the gate error probability is below a certain threshold, a reduced gate error probability is attained.*
2) *Our solution is capable of encoding quantum information without the need for encoding circuits, which are inherently error-prone. We achieve this ambitious objective by proposing an additional syndrome decoding step, which prepares a code space containing the same legitimate codewords. This encoderless scheme relies on a fault-tolerant circuit and as a further benefit, it requires fewer gates than the family of common state preparation techniques [1], [2].*
3) *Using the proposed encoderless scheme, upper bounds of the qubit decoherence probability and gate error are derived that define the conditions of constructing an output state having an error rate of* 10^{-5}.

The structure of the paper is described as follows. First the Steane code is introduced in Section I-B. Then Section I-C to I-D portray the fault-tolerant implementation of a stabilizer measurement, while Section I-E elaborates on the stabilizer measurements applied to arbitrary input states. The encoderless codes advocated are introduced in Section II using the rudimentary example of the repetition code. This is then extended to Steane's code [16] in Section III, followed by our results recorded for imperfect gates. Finally, our encoderless scheme is extended to state preparation protocols in Section IV, where qubit decoherence probability and gate error probability bounds are derived.

A. INTRODUCTION TO QECC

Due to the small scale of near-intermediate-scale-quantum (NISQ) devices [14], there has been great interest in solutions that do not require the qubit overheads of QECC. However, despite the progress made in improving gate fidelity and qubit coherence times, QECC will be necessary to mitigate component errors in large-scale practical quantum algorithms. A QECC attaches redundancy to quantum information in such a way that the individual qubit errors can be corrected without corrupting the logical qubit state. However, the encoding and decoding circuits are built by individual quantum gates. If these components are error-prone it will increase the qubit error probability, hence leading to an even more grave corruption of the data qubits. Therefore constructing a QECC that has fault tolerant circuitry is crucial for creating quantum solutions.

There has been a lot of progress in QECC since its inception by Shor in 1995, where he conceived the $\frac{1}{9}$-rate code [17]. This was based on the repetition code, and has the ability to correct both bit and phase-errors. Shor's code motivated the design of Calderbank-Shor-Steane (CSS) codes [18], [19], which exploit the properties of classical linear block codes, providing a more general framework to correct both bit and phase-errors than Shor's code. As a further development, using the [7, 4, 3] Hamming code the $\frac{1}{7}$-rate Steane code was devised, which can correct a single arbitrary qubit error [19]. This code rate was then further improved in [20], [21], showing that a $\frac{1}{5}$-rate code was the shortest possible codeword length capable fo correcting a single qubit error. Gottesman then outlined the quantum stabilizer code (QSC) formalism in his PhD thesis [22] for providing a general framework capable of further improving the efficiency of QECCs [23]. The benefit of QSCs is that their construction is not restricted to CSS codes, therefore their inception sparked off the development of a wide variety of QECCs (see [24]). Since the focus of this paper is on the $\frac{1}{7}$-rate Steane code, let us introduce this in the next section.

B. TRADITIONAL STEANE CODE

Let us first briefly introduce the Steane Code, whilst mentioning that its tutorial description be found in [3], [25]. The Steane code belongs to the family of Calderbank-Shor-Steane (CSS) code, which is a general construction using a pair of classical linear block codes $\mathcal{C}_1$ and $\mathcal{C}_2$ where $\mathcal{C}_2 \subset \mathcal{C}_1$. The Steane code is a dual-containing CSS code obeying the property of $\mathcal{C}_2 = \mathcal{C}_1^{\perp}$. This is constructed using the [7, 4, 3] classical Hamming code. Since this is a single bit-error correcting code, it leads to a single-qubit error correcting quantum code having the parameters of [7, 1, 3]. Therefore a single data qubit is encoded into 7 physical qubits. The encoded states can be prepared by the traditional Steane encoding circuit[3] $\mathcal{V}$ shown in Figure 1. This is applied to the unknown state $|\psi\rangle = \alpha|0\rangle + \beta|1\rangle$ and $(n-k)$ auxiliary qubits as follows

$$|\overline{\psi}\rangle = \mathcal{V}(|\psi\rangle \otimes |0\rangle^{\otimes(n-k)}) = \alpha|\overline{0}\rangle + \beta|\overline{1}\rangle, \tag{1}$$

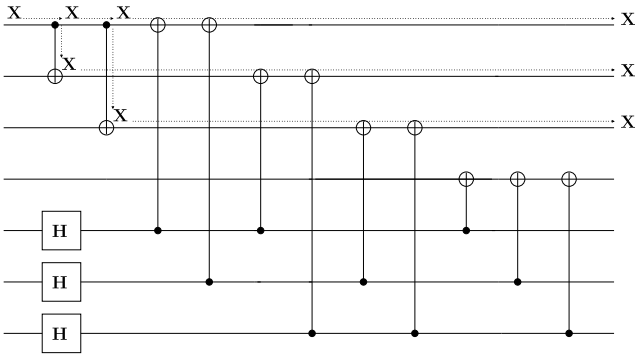

FIGURE 1. Traditional Steane encoding circuit suffering from *X* error proliferation [15].

where we have

$$\begin{aligned}|\overline{0}\rangle = \frac{1}{\sqrt{8}}\big[&|0000000\rangle + |1010101\rangle + |0110110\rangle \\ &+ |1100110\rangle + |0001111\rangle + |1011010\rangle \\ &+ |0111100\rangle + |1101001\rangle\big]\end{aligned} \tag{2}$$

and

$$\begin{aligned}|\overline{1}\rangle = \frac{1}{\sqrt{8}}\big[&|1111111\rangle + |0101010\rangle + |1001100\rangle \\ &+ |0011001\rangle + |1110000\rangle + |0100101\rangle \\ &+ |1000011\rangle + |0010110\rangle\big].\end{aligned} \tag{3}$$

The Steane code stabilizers are as follows

$$\begin{aligned}K_1 &= IIIXXXX, \\ K_2 &= XIXIXIX, \\ K_3 &= IXXIIXX, \\ K_4 &= IIIZZZZ, \\ K_5 &= ZIZIZIZ, \\ K_6 &= IZZIIZZ.\end{aligned} \tag{4}$$

which forms $\hat{\mathcal{S}} = \{K_i\}$.

The stabilizers are applied via a syndrome extraction circuit, whereby additional ancilla qubits are coupled to the codeword state. This is done by applying a series of two-qubit gates with a pre-determined location according to the operators in Eq. (4). The measurement of the ancilla qubit extracts the syndrome outcome, which illustrates the outcome of the relevant parity checks of the physical codeword qubits. Therefore if the data qubits contain a single qubit error, the location of this error will be indicated by the combination of classical bit measurement outcomes. A correction can then be applied in order to return the corrupted word to a legitimate codeword state. Likewise, if the data is error-free, the all-zero syndrome will be extracted, indicating that no error correction operation is necessary.

C. FAULT-TOLERANT STABILIZER

Figure 2 shows the circuit construction of the Steane code stabilizer of $K_1 = IIIXXXX$ [16], in which a single bit-flip error on the ancilla qubit is propagated to $t > 1$ errors in the data qubits. This is because the bit-flip error on the control qubit of the first CNOT gate leads to the application of the NOT gate ($\bigoplus$) on the target qubit. Moreover, the control error is not deleted by the action of the logic gate, since the CNOT is a reversible gate. This means that the input information is preserved at the output of the logic gate. Therefore the bit-flip error on the control qubit is input into the second, third and fourth CNOT gates. What began as a single error is spread across the qubit register to $t = 4$ errors. Since the Steane code has a minimum distance of $d = 3$ this circuit construction is not fault-tolerant.

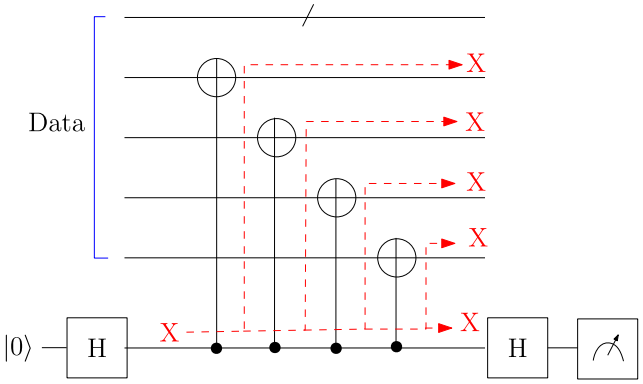

FIGURE 2. Non-fault-tolerant implementation of the Steane code stabilizer $K_1 = IIIXXXX$ [2].

This error-proliferation phenomenon is a general property of all stabilizer circuits obeying the architecture of Figure 2. Fortunately, fault-tolerant schemes do exist, such as the one developed by

Peter Shor in [5] which is described in this section. However, in most practical cases, a more efficient scheme would

[3]The flow of time in a quantum circuit diagram is from left to right. The qubit register is represented from top to bottom, where the spatial connectivity required is indicated by the qubits coupled by two-qubit gates. Where the outcome of a circuit block is input to another it is indicated by solid a line and arrows.

be employed such as those in [16], [26], [27], which require reduced qubit overheads [10], [28], [29].

Figure 3 shows the fault-tolerant implementation of the $K_1 = IIIXXXX$ Steane code stabilizer. The general idea of the scheme is that the ancilla qubit is replaced by an error-free *superimposed state* [5]. Replacing the ancilla with a state that is error-free ensures that less qubit errors are propagated to the data qubits by the gates coupling the ancilla and the data. An N-qubit superimposed state is chosen, where N is the same as the number of CNOT gates in the traditional stabilizer. This is equivalent to the weight[4] of the stabilizer, so for example we have $N = \text{wt}(IIIXXXX) = 4$. Replacing an ancilla qubit by an ancilla state means that the CNOT gates in the stabilizer can be applied to the ancilla relying on the same circuit construction as a transversal CNOT gate. This inherits the fault-tolerant properties of the transversal CNOT gates, see [3], [15]. The transversal construction ensures that there are no scenarios whereby a single qubit error can result in increased-weight errors at the circuit's output. This is because there are no qubits either in the data or in the ancilla state that are connected by more than a single CNOT connection.

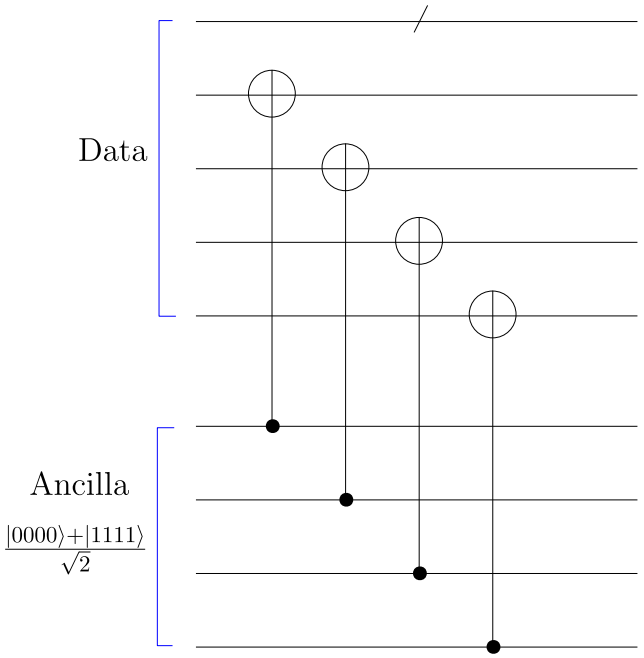

FIGURE 3. Fault-tolerant implementation of the Steane code stabilizer $K_1 = IIIXXXX$ [2].

The aim of the stabilizer is to copy the error information into the ancilla qubit without directly measuring the data qubits. To do this, the ancilla must be in an equi-probable superposition so that the eigenstate of the data is encapsulated in a ± 1 phase difference. Figure 2 shows that a Hadamard gate is applied to the ancilla qubit before the stabilizer. Therefore the stabilizer circuit puts the ancilla qubit into the state $\frac{(|0\rangle+|1\rangle)}{\sqrt{2}}$ before applying the controlled-K gate[5]. This state is extended in the fault-tolerant circuit construction to the following N-qubit superimposed state

$$\frac{(|00\ldots00\rangle + |11\ldots11\rangle)}{\sqrt{2}}. \tag{5}$$

Then the ± 1 eigenstate in the data is passed to the ancilla state $|00\ldots00\rangle \pm |11\ldots11\rangle$, where the ± 1 phase difference can be detected by a measurement. A fault-tolerant way to do this measurement is to apply a Hadamard gate to all N qubits. This is because we see that

$$H^{\otimes N}\frac{(|00\ldots00\rangle + |11\ldots11\rangle)}{\sqrt{2}} = |i\rangle^{\otimes N} \tag{6}$$

has an even weight, when the phase difference is positive and odd weight when the phase difference is negative. It is necessary to use a superimposed state in the ancilla rather than simply duplicating the ancilla qubit N times because in this case the ancilla state would be $|+\rangle^{\otimes N}$, but this will not work because the eigenstate of the data is determined by directly measuring each qubit of the ancilla state.

D. SUPERIMPOSED STATE PREPARATION

This section describes how the ancilla state is prepared without an error. The scheme to do this was developed by Shor in [5]. The circuit shown in Figure 4 prepares the corresponding superimposed state. This circuit is not itself fault-tolerant, but the superimposed state is part of a fault-tolerant stabilizer implementation [5]. An error-free superimposed state is determined by detecting errors using a parity check and an extra ancilla qubit. For example, an $N = 4$ qubit example of a superimposed state is

$$\frac{(|0000\rangle + |1111\rangle)}{\sqrt{2}}. \tag{7}$$

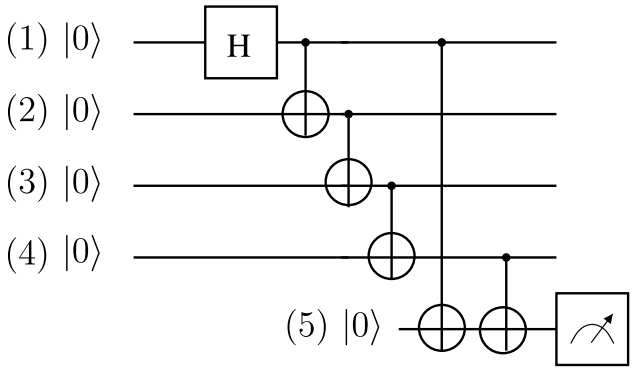

FIGURE 4. Circuit to construct a superimposed state [30].

This state represents an equi-probable superposition of equally weighted N-qubit all-zero and all-one vectors. The qubit locations of the parity check CNOT gates should be chosen randomly and repeated until the state can be deemed

[4]The weight wt(S) of a quantum operator S is defined as the number of qubits that differ from the identity operator. Therefore wt(XIZ) = 2.

[5]An arbitrary stabilizer K can be implemented as a controlled-K gate [2].

error-free [4], [5]. For example, let us assume that an XI error is imposed by the CNOT gate connecting qubits (2) and (3) in Figure 4. This will result in the following state

$$\frac{(|0100\rangle + |1011\rangle)}{\sqrt{2}}. \tag{8}$$

In this case there is an error on qubit (2) which will be detected by a parity check measurement between different circuit locations to that shown in Figure 4. A gate error which results in the state

$$\frac{(|0010\rangle + |1101\rangle)}{\sqrt{2}} \tag{9}$$

is detected by another parity check combination. Likewise, other error combinations include

$$\frac{(|1000\rangle + |0111\rangle)}{\sqrt{2}}$$
$$\frac{(|1100\rangle + |0011\rangle)}{\sqrt{2}}$$
$$\frac{(|0001\rangle + |1110\rangle)}{\sqrt{2}},$$

which can be detected by measuring the parity check ancilla qubit (marked (5) in Figure 4). If a qubit error is propagated to all $N = 4$ qubits, the resultant superimposed state remains unaffected. Therefore, the specific location of the parity check in Figure 4 will detect the most common error, where the first and last qubits are not similar. If the measurement outcome indicates that the ancilla is in the $|0\rangle$ state, then the superimposed state has been prepared without error. If by contrast a $|1\rangle$ state is measured, this indicates that the state prepared should be thrown away and the process must be re-initialized.

The above-mentioned state construction ensures that there are no X errors in the ancilla qubits, since error detection is used for spotting and throwing away the states with bit-flip errors. Therefore there will be no bit-flip error proliferation imposed on the data qubits. However, there are a pair of scenarios that may results in an incorrect syndrome measurement. A single phase error during the superimposed state preparation results in the phenomenon that the ancilla state $|00\ldots00\rangle - |11\ldots11\rangle$ forces the ± 1 eigenvalues to switch places. This would result in an incorrect syndrome measurement. The second scenario is that a gate failure in the CNOT gates constructing the syndrome operator would also result in an incorrect measurement outcome.

To combat this problem, the full stabilizer procedure must be repeated for example three times [31]. Then a majority vote is taken to determine the final stabilizer value but the third stabilizer measurement is only necessary when the first two measurement outcomes differ. This means that an incorrect stabilizer result will occur at a probability order of p^2 where p is the probability of a component error, because two of the stabilizer implementations must simultaneously contain a component error for the majority vote to conclude the absence of errors due to a pair of errors. Therefore in the best case scenario, a single syndrome measurement requires an additional 10 ancilla qubits assuming that the superimposed state is prepared without error first time and the first as well as second syndrome measurements match. However, it is possible for this to become more than doubled, because multiple superimposed states may have to be produced to distill a single error free version and this must be done for each repeated stabilizer measurement. Therefore the extent of the qubit overheads is determined by the efficiency of creating an error-free ancilla state. For the full l = n-k = 6 Steane code stabilizer set it is not unreasonable to expect more than 60 additional ancilla qubits which is in stark contrast to the 6 required for the non-fault-tolerant scheme.

E. STABILIZER MEASUREMENTS WITH ARBITRARY INPUT STATE

This sub-section follows from the section entitled as *Non-Destructive Operator Measurement* in [3]. It is useful to determine the effect of an operator measurement in Figure 5 for any arbitrary input state $|\psi\rangle$ [32].

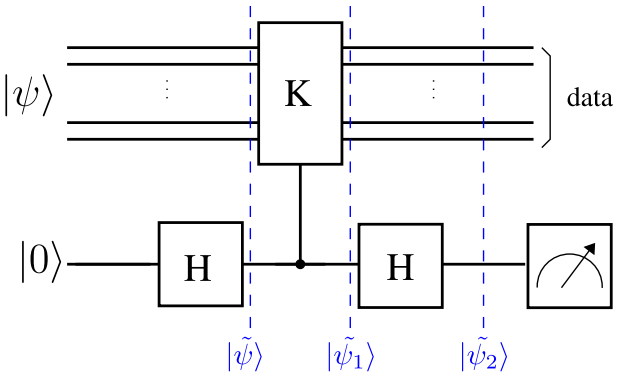

FIGURE 5. Measurement of an arbitrary single stabilizer operator K. (from [3]).

Let us describe the transformation of the circuit in Figure 5 step-by-step for input state $|\psi\rangle$. The first Hadamard gate in the circuit in Figure 5 has the transformation described by

$$|\psi\rangle|0\rangle \xrightarrow{\text{H}} |\psi\rangle|+\rangle = \frac{1}{\sqrt{2}}\Big[|\psi\rangle|0\rangle + |\psi\rangle|1\rangle\Big] = |\tilde{\psi}\rangle. \tag{10}$$

The controlled-K gate applies the K operator only when the ancilla qubit is in the $|1\rangle$ state [2]. Therefore the controlled-K gate has the transformation

$$|\tilde{\psi}\rangle \rightarrow \frac{1}{\sqrt{2}}\Big[|\psi\rangle|0\rangle + K|\psi\rangle|1\rangle\Big] = |\tilde{\psi}_1\rangle. \tag{11}$$

and we arrive at an expression for $|\tilde{\psi}_1\rangle$. After applying another Hadamard gate after $|\tilde{\psi}_1\rangle$ we get

$$\frac{1}{\sqrt{2}}\Big[|\psi\rangle|0\rangle + K|\psi\rangle|1\rangle\Big] \xrightarrow{\text{H}} \frac{1}{\sqrt{2}}\Big[|\psi\rangle|+\rangle + K|\psi\rangle|-\rangle\Big] = |\tilde{\psi}_2\rangle \tag{12}$$

Expanding Eq. (12) gives the state of the system before the ancilla measurement

$$|\tilde{\psi}_2\rangle = \frac{1}{2}\Big[(|\psi\rangle + K|\psi\rangle)|0\rangle + (|\psi\rangle - K|\psi\rangle)|1\rangle\Big]. \quad (13)$$

Let us now describe the effect of this circuit using the simple example of the repetition code. In this case the input state is a superposition of error-free legitimate code word states. Consider the circuit in Figure 5 with $|\psi\rangle = \alpha|000\rangle + \beta|111\rangle$ the stabilizer operator $K_1 = ZZI$. Note that this stabilizer leaves the legitimate code word state $|\psi\rangle$ unchanged, therefore $K_1|\psi\rangle = |\psi\rangle$. Then Eq.(13) is shown to be

$$\frac{1}{2}\Big[(|\psi\rangle + |\psi\rangle)|0\rangle + (|\psi\rangle - |\psi\rangle)|1\rangle\Big] = |\psi\rangle|0\rangle. \quad (14)$$

Therefore in the event that a legitimate codeword state is the input, the outcome of the ancilla measurement is 0.

Let us consider the scenario that the input state is a superposition of illegitimate code word states, for example $|\psi\rangle = \alpha|100\rangle + \beta|011\rangle$. This state contains a single qubit error and therefore it can be corrected by the repetition code, so $K_1|\psi\rangle = -|\psi\rangle$. Within these restrictions Eq. (13) becomes

$$\frac{1}{2}\Big[(|\psi\rangle + (-|\psi\rangle))|0\rangle + (|\psi\rangle - (-|\psi\rangle))|1\rangle\Big] = |\psi\rangle|1\rangle. \quad (15)$$

Therefore in the event that a correctable error is input, then the outcome of the ancilla measurement becomes 1.

In the case where the input state is a superposition of ± 1 eigenstates, the measurement of the stabilizer operator will have the effect of 'projecting' the data into either of the ± 1 eigenstates [2], [32]. The quantum stabilizer measurement is designed so that the data is entangled with the ancilla, and the measurement of the ancilla projects the data into a ± 1 eigenstate of the stabilizer.

Let us now elaborate on a scenario that explains this in more detail. Consider Figure 5 when $|\psi\rangle = \alpha|000\rangle + \beta|100\rangle$, namely a superposition of legitimate and illegitimate codewords. When K_1 is applied to this state, the outcome is $K_1|\psi\rangle = \alpha|000\rangle - \beta|100\rangle$. Substituting this into Eq.(13) and simplifying it further leads to

$$\alpha|000\rangle|0\rangle + \beta|100\rangle|1\rangle. \quad (16)$$

if a 1 is measured in the ancilla, we can guarantee the data now resides in the state $|100\rangle$. The ancilla measurement triggers an error correction operation, which then returns the data to a legitimate code word state, in this case $|000\rangle$. Likewise is a 0 is measured in the ancilla it indicates the data now resides in the $|000\rangle$ state. It can be said that the stabilizer measurement 'projects' the input information into a legitimate or illegitimate codeword state [2], [32].

Then referring back to Eq. (13), in general when the ancilla qubit of Figure 5 is in the state $|0\rangle$, the data qubits are described by

$$|\tilde{\psi}_2\rangle = \frac{1}{2}\big(|\psi\rangle + K|\psi\rangle\big), \quad (17)$$

which is the $+1$ eigenstate of K. Likewise, when a $|1\rangle$ is measured in the ancilla, the state of the data qubits is given by

$$\frac{1}{2}\big(|\psi\rangle - K|\psi\rangle\big), \quad (18)$$

which is the -1 eigenstate of K. These equations will be referred back to when determining the effect of the measurement of a stabilizer for an arbitrary input state of $|\psi\rangle$.

II. ENCODERLESS QECC

Section IV will outline a scheme whereby a known state can be prepared without the application of the traditional encoder [32]. This can be achieved by preparing an initial input state that is understood to evolve to the intended known encoded state with the application of syndrome decoding. However it is not yet understood if this approach can be pursued for encoding an unknown state [33], which we have no prior information concerning the probability α and β before encoding. This section proposes a scheme for solving this problem. In practice traditional unitary encoding circuits must be applied for encoding an unknown state.

The scheme operating in the face of combined gate error and quantum bit error channel model presented in [3] requires the gate error P_g to be an order of magnitude lower than the quantum bit decoherence probability P_e. This is the limitation imposed by the gate error in the encoding circuit. The error rate of the encoding circuit is upper bounded by single gate errors, therefore introducing an error rate on the order of $\mathcal{O}(P_g)$ after syndrome decoding. This section presents a scheme which does not require encoding circuits, therefore reducing the probability of gate error in the encoder the order of $\mathcal{O}(P_g^2)$ that can nevertheless encode an unknown state.

A. ENCODERLESS REPETITION CODE

Again quantum information can be protected without an encoding circuit by preparing a legitimate and illegitimate codeword states in a superposition and then applying syndrome decoding to transform this to valid codeword states. Let us now explore this idea in more detail. Firstly, let us compare the repetition encoded state of

$$|\overline{\psi}\rangle = \alpha|\overline{0}\rangle + \beta|\overline{1}\rangle = \alpha|000\rangle + \beta|111\rangle, \quad (19)$$

to the state produced by the circuit that replaces the encoder by a pair of Hadamard gates, as shown in Figure 6. After applying both Hadamard gates to the unknown input state of $|\psi\rangle = \alpha|0\rangle + \beta|1\rangle$, the system is in the state

$$|\tilde{\psi}\rangle = (\alpha|0\rangle + \beta|1\rangle) \otimes \left(\frac{|0\rangle + |1\rangle}{\sqrt{2}}\right) \otimes \left(\frac{|0\rangle + |1\rangle}{\sqrt{2}}\right). \quad (20)$$

Expanding this gives

$$|\tilde{\psi}\rangle = \underline{\alpha|000\rangle} + \alpha|001\rangle + \alpha|010\rangle + \alpha|011\rangle + \underline{\beta|111\rangle} + \beta|110\rangle + \beta|101\rangle + \beta|100\rangle. \quad (21)$$

The vectors that overlap with the state shown in Eq. (19) are underlined.

The vectors that are not underlined must be corrected to one of the valid code word states in Eq. (19). Additionally, the coefficients α or β have to be consistent with the encoded state of $\alpha|\bar{0}\rangle + \beta|\bar{1}\rangle$. For example, the vector $\beta|100\rangle$ must be corrected to $\beta|111\rangle$. This can be done by measuring the traditional repetition code stabilizers $K_1 = ZZI$ as well as $K_2 = ZIZ$ and then carrying out the recovery operations shown in Table 1. To elaborate these operations are similar to those based on the traditional repetition code (see [34]) except that when the ancilla qubits are in state $|11\rangle$, the bit flip correction is applied to both the second and third data qubits X_2X_3 ensuring that

$$\alpha|011\rangle + \beta|100\rangle \rightarrow \alpha|000\rangle + \beta|111\rangle. \tag{22}$$

TABLE 1. Error recovery operators $\widehat{\mathcal{R}}$ for the encoderless [3, 1, 3] Repetition code.

$\widehat{\mathcal{R}}$	$\|\text{data}\rangle\|\text{ancilla}\rangle$
III	$(\alpha\|000\rangle + \beta\|111\rangle)\|00\rangle$
IIX	$(\alpha\|001\rangle + \beta\|110\rangle)\|01\rangle$
IXI	$(\alpha\|010\rangle + \beta\|101\rangle)\|10\rangle$
IXX	$(\alpha\|011\rangle + \beta\|100\rangle)\|11\rangle$

This is necessary because if the traditional single qubit correction X_1 was made, this would result in the state $\alpha|111\rangle + \beta|000\rangle$. In this case the coefficients are the wrong way around therefore the result is not consistent with Eq. (19). The aim of the scheme in Figure 6 is to ensure that $|\overline{\psi}\rangle = \alpha|000\rangle + \beta|111\rangle$.

Let us now describe the operations in Table 1 is discovered. The input state of Eq. (21) evolves under the measurement of the stabilizers K_1 and K_2 according to Eq. (17) and Eq. (18), yielding

$$|\tilde{\psi}_2\rangle = \frac{1}{2}\big(|\psi\rangle + K|\psi\rangle\big) \quad |\tilde{\psi}_2\rangle = \frac{1}{2}\big(|\psi\rangle - K|\psi\rangle\big). \tag{23}$$

Let us consider the example that a $|0\rangle$ is measured in both the ancilla qubits each described by Eq. (17). First, $|\tilde{\psi}\rangle \rightarrow |\tilde{\psi}_1\rangle$ when K_1 of Figure 6 is measured, given by

$$|\tilde{\psi}_1\rangle = = \frac{1}{2}\big(|\tilde{\psi}\rangle + ZZI|\tilde{\psi}\rangle\big) = \alpha|000\rangle + \alpha|001\rangle + \beta|111\rangle + \beta|110\rangle.$$

This state is then input to the measurement of the K_2 stabilizer. A $|0\rangle$ is also measured in the second ancilla qubit, giving

$$|\tilde{\psi}_2\rangle = \frac{1}{2}\big(|\tilde{\psi}_1\rangle + ZIZ|\tilde{\psi}_1\rangle\big) = \alpha|000\rangle + \beta|111\rangle. \tag{24}$$

This shows that the encoded state $|\overline{\psi}\rangle$ is recovered without having to apply an error correction operation $\widehat{\mathcal{R}}$.

Let us now check the effect of measuring the $|01\rangle$ ancilla states. After the K_1 stabilizer is applied, the system is in the same state, as described in Eq. (24). Then the second measurement of the K_2 stabilizer results in the $|1\rangle$ state in the ancilla qubit. This is described by Eq. (18), so in this case we have

$$|\tilde{\psi}_2\rangle = \frac{1}{2}\big(|\tilde{\psi}_1\rangle - ZIZ|\tilde{\psi}_1\rangle\big) = \alpha|001\rangle + \beta|110\rangle \tag{25}$$

and a bit flip recovery operation X_3 will return the state to $|\overline{\psi}\rangle$. The same calculation can be done for the other two scenarios listed in Table 1.

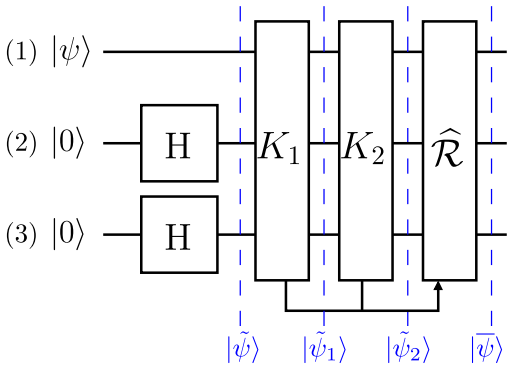

FIGURE 6. Encoderless [3, 1, 3] Repetition Code.

Let us see the effect of measuring the $|10\rangle$ ancilla states. After the K_1 stabilizer is applied the system is in

$$|\tilde{\psi}_1\rangle = \frac{1}{2}\big(|\tilde{\psi}\rangle - ZZI|\tilde{\psi}\rangle\big) = \alpha|010\rangle + \alpha|011\rangle + \beta|101\rangle + \beta|100\rangle. \tag{26}$$

The $|0\rangle$ state is measured in the second ancilla qubit, giving

$$|\tilde{\psi}_2\rangle = \frac{1}{2}\big(|\tilde{\psi}_1\rangle + ZIZ|\tilde{\psi}_1\rangle\big) = \alpha|010\rangle + \beta|101\rangle. \tag{27}$$

hence the $\widehat{\mathcal{R}} \equiv IXI$ correction operation recovers $|\overline{\psi}\rangle$. Similarly, if the $|11\rangle$ ancilla state is measured, we have

$$|\tilde{\psi}_2\rangle = \frac{1}{2}\big(|\tilde{\psi}_1\rangle - ZIZ|\tilde{\psi}_1\rangle\big) = \alpha|011\rangle + \beta|100\rangle \tag{28}$$

and the $\widehat{\mathcal{R}} \equiv IXX$ correction operation recovers $|\overline{\psi}\rangle$.

Furthermore, any single Hadamard gate error acts trivially on the state $|\tilde{\psi}\rangle$. So even though at this step in the circuit the state is not strictly encoded in the state $|\overline{\psi}\rangle$, the scheme is still robust against the gate errors of its preparation circuits. For example, a Hadamard gate error on the middle qubit can be described by IXI for the bit-flip channel $\mathcal{E}(.)$. The channel output is described by

$$\mathcal{E}(|\tilde{\psi}\rangle) = IXI|\tilde{\psi}\rangle = |\tilde{\psi}\rangle, \tag{29}$$

where $|\tilde{\psi}\rangle$ is given by Eq. (21). This error takes one vector state in the superposition state $|\tilde{\psi}\rangle$ to another and preserves the coefficients α and β. Similarly a Hadamard gate error on qubit (3) has the same effect, namely $IIX|\tilde{\psi}\rangle = |\tilde{\psi}\rangle$. In fact, two simultaneous Hadamard gate errors occurring with probability P_g^2 is also trivial, since we have $IXX|\tilde{\psi}\rangle = |\tilde{\psi}\rangle$. Therefore no possible gate error combination suffers from an error that cannot be corrected by the measurement of $\widehat{\mathcal{S}}$.

Note that the error correction operations must still be applied. Since the state in Eq. (21) consists of only ± 1 eigenstates of $\widehat{\mathcal{S}}$, the application of $\widehat{\mathcal{R}}$ results in $|\tilde{\psi}\rangle \rightarrow |\overline{\psi}\rangle$, as seen in Figure 6. In simple terms, the input state $|\tilde{\psi}\rangle$ is in a superposition of the code word states and correctable errors. This state is carefully designed in such a way that the unknown coefficients α and β are preserved after $\widehat{\mathcal{R}}$. So the unknown state $|\psi\rangle$ effectively ends up in the encoded state $|\overline{\psi}\rangle$ by the application of $\widehat{\mathcal{S}}$ and $\widehat{\mathcal{R}}$.

B. ENCODERLESS TRANSVERSAL CNOT GATE

The encoderless scheme depicted in Figure 7 applies the transversal CNOT gate $\overline{U}_f$ to the control and target qubits $|\phi_1\rangle$ and $|\phi_2\rangle$. Both qubits are separately prepared in the partially encoded state in Eq. (21) with the addition of $n-k = 2$ ancilla qubits. In this scheme the original repetition code recovery operation $\mathcal{R}$ is applied, therefore FER improvements are expected with the aid of $\widehat{\mathcal{R}}$. This scheme applies the following transformation

$$\overline{U}_f(|\phi_1\rangle|++\rangle|\phi_2\rangle|++\rangle) \xrightarrow{\widehat{\mathcal{S}},\mathcal{R}} \overline{U}_f(|\overline{\phi_1}\rangle|\overline{\phi_2}\rangle), \quad (30)$$

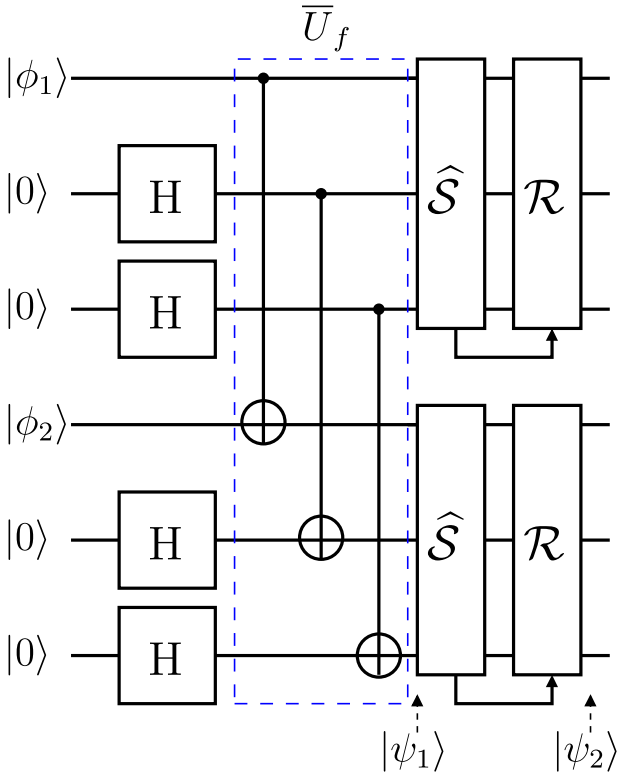

FIGURE 7. Encoderless transversal CNOT using the [3, 1, 3] Repetition Code.

so that after syndrome decoding the control and target states $|\overline{\phi_1}\rangle$ and $|\overline{\phi_2}\rangle$ are encoded as well as transformed by the CNOT gate. Syndrome decoding is applied after the transversal CNOT gate since $\overline{U}_f$ commutes with $\widehat{\mathcal{S}}$, see [3].

C. FER WITHOUT ENCODER

Figure 8 shows the upper and lower bound of the FER to be derived in this section for the encoderless scheme with a channel model, whereby each CNOT and Hadamard gate is a potential source of error location with a gate error probability of P_g. This section contrasts our simulation results to these bounds. The FER before decoding at position $|\psi_2\rangle$ of Figure 7 is

$$FER_2 = 7P_g + 21P_g^2 \quad (31)$$

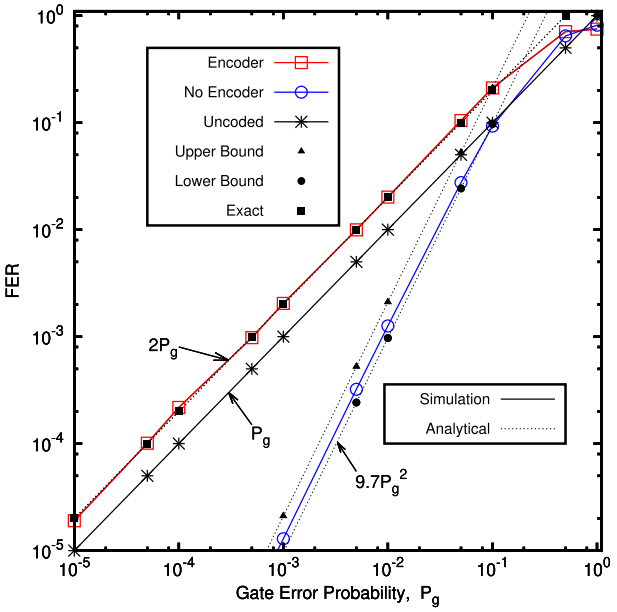

FIGURE 8. Transversal CNOT gate in the bit-flip channel with [3, 1, 3] repetition code with and without the traditional encoding circuit.

More explicitly, since this circuit construction is fault-tolerant, the term $7P_g$ can be ignored as any single gate error can be corrected by the syndrome decoders. Therefore it is only necessary to consider the proportion of errors occurring owing to a pair of simultaneous gate errors. Given 4 Hadamard gates and 3 CNOT gates in the circuit there are 21 combinations of two simultaneous gate errors, so Eq. (31) can be re-written as

$$FER_2 = \eta P_g^2 < 21P_g^2. \quad (32)$$

Therefore the upper bound of the FER marked with a triangle in Figure 8 is

$$FER^{\text{UPPER}} = 21P_g^2. \quad (33)$$

The value of η in Eq. (31) is found by considering the probability that two simultaneous gate errors can be corrected, and subtracting this probability from $21P_g^2$.

There are three general categories that the 21 combinations of two simultaneous gate errors may take:

- Two simultaneous Hadamard gate errors (6 combinations),

- Two simultaneous CNOT gate errors (3 combinations),
- Simultaneous CNOT gate and Hadamard gate error (12 combinations),

These will be considered in each subsection that follows.

1) TWO SIMULTANEOUS HADAMARD GATE ERRORS

Let us start with analyzing the six combinations of two simultaneous Hadamard gate errors, which contributes $6P_g^2$ to FER_2. Firstly, a single qubit gate objected to the bit flip channel simply incurs an X error with a probability of P_g (namely the gate error). Therefore more than qubit errors will be encountered, only when two Hadamard gates in the same encoded block impose an error in either the top or the bottom syndrome decoder of Figure 7 This only occurs in 2 out of the 6 two-Hadamard gate error combinations. Then two simultaneous Hadamard gate errors can be corrected with a probability of $4P_g^2$ giving $\eta P_g^2 < 17P_g^2$.

2) TWO SIMULTANEOUS CNOT GATE ERRORS

Furthermore, there are only three scenarios, where a pair of CNOT gates have an error simultaneously, which contributes a probability of $3P_g^2$ to FER_2. When we consider the two-qubit gate bit-flip error event of (IX, XI, XX) two CNOT gates suffer from an error, this gives 9 combinations, each occurring with a probability of $\frac{P_g}{3} \cdot \frac{P_g}{3}$. Each combination is listed in Table 2 and visualized in Figure 9. There are only two combinations that result in a single qubit error being input into the top and bottom syndrome decoder in Figure 9. Therefore each time when two CNOT gates have an error simultaneously this may be corrected with a probability of $\frac{2P_g^2}{9}$. Then accounting for all three 'two-simultaneous-CNOT-gate-error' combinations gives $\eta P_g^2 < 16.3P_g^2$.

TABLE 2. Combinations of two simultaneous CNOT gate error in the bit-flip channel.

CNOT 1	CNOT 2	Correctable
IX	IX	N
IX	XI	Y
IX	XX	N
XI	IX	Y
XI	XI	N
XI	XX	N
XX	IX	N
XX	XI	N
XX	XX	N

3) SIMULTANEOUS CNOT GATE AND HADAMARD GATE ERROR

Next there are twelve scenarios, where a Hadamard and a CNOT gate have an error simultaneously. There are two ways this could happen. Let us start with the simplest case namely which a Hadamard gate error is input to the CNOT gate,

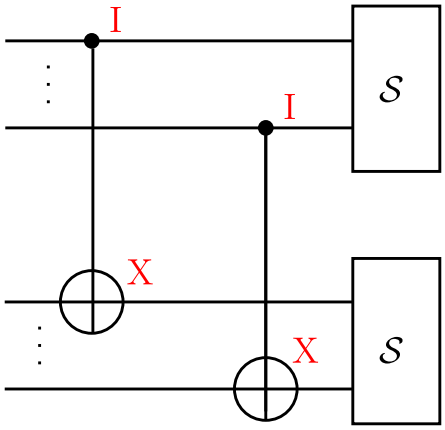

FIGURE 9. ***IX*** **error on both CNOT 1 and CNOT 2 resulting in two qubit error input into the bottom encoder.**

as shown in Figure 10. In this case there may be no more than one error entered into each syndrome decoder in Figure 10. This is because the transversal CNOT gate will not proliferate the input error to more than one error. Additionally, the CNOT gate error cancels the propagated Hadamard gate error. There are four scenarios, where a Hadamard gate is applied to a qubit before it is input to a CNOT gate - therefore we have $\eta P_g^2 < 12.3P_g^2$.

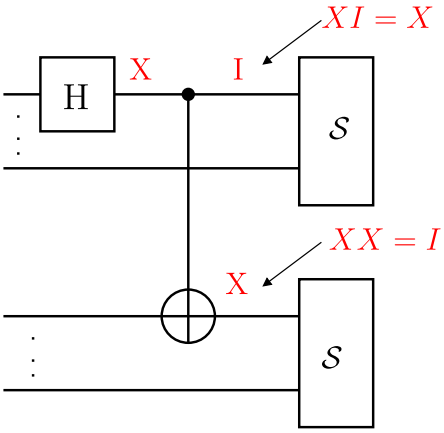

FIGURE 10. **A scenario where one error event cancels another. A Hadamard gate incurs an** ***X*** **error that is subsequently input to the control qubit of a CNOT gate, which itself has incurred an** ***IX*** **error.**

The last 8 scenarios are where the Hadamard gate error is at a location that is either in an encoded block, but its output is not entered into that specific CNOT gate, which has a simultaneous gate error, as shown in Figure 11. Table 3 shows that with a probability of $\frac{P_g^2}{3}$ this combination will not incur a [3, 1, 3] frame error. This is valid for all 8 combinations. Hence the total associated probability is $\frac{8P_g^2}{3}$. Therefore finally we get $\eta P_g^2 < 9.7P_g^2$, which gives $\eta \approx 9.7$ in Eq. (31). Consequently the lower bound marked with a circle in Figure 8 is given by

$$FER^{\text{LOWER}} = 9.7P_g^2. \tag{34}$$

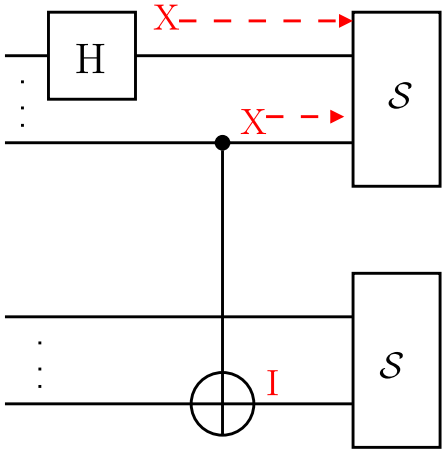

FIGURE 11. *X* error imposed on a Hadamard gate occurring in the same encoded block as the control qubit error of a CNOT associated with an *XI* error.

TABLE 3. Combinations of a Hadamard gate error in the same encoded block as the target qubit of a simultaneous CNOT gate error in the bit flip channel. See Figure 11.

H	CNOT	Correctable
X	IX	Y
X	XI	N
X	XX	N

Having introduced the basis of the encoderless scheme, let us now focus our attention on the more practical Steane code in the next section.

III. ENCODERLESS STEANE CODE

A. ENCODERLESS STEANE CODE

The scheme of Figure 12 replaces the traditional $n = 7$ qubit unitary encoding circuit $\mathcal{V}$ seen in Figure 1. Ordinarily, the encoder $\mathcal{V}$ is applied to both the unknown state $|\psi\rangle = \alpha|0\rangle + \beta|1\rangle$ and to $(n-k)$ auxiliary qubits as follows [34]

$$|\overline{\psi}\rangle = \mathcal{V}(|\psi\rangle \otimes |0\rangle^{\otimes(n-k)}). \tag{35}$$

This achieves the encoded state,

where we have:

$$\begin{aligned}|\overline{\psi}\rangle = \frac{\alpha}{\sqrt{8}}\big[&|0000000\rangle + |1010101\rangle + |0110011\rangle \\ &+ |1100110\rangle + |0001111\rangle + |1011010\rangle \\ &+ |0111100\rangle + |1101001\rangle\big] \\ &+ \frac{\beta}{\sqrt{8}}\big[|1111111\rangle + |0101010\rangle + |1001100\rangle \\ &+ |0011001\rangle + |1110000\rangle + |0100101\rangle \\ &+ |1000011\rangle + |0010110\rangle\big].\end{aligned} \tag{36}$$

Let us compare this to the state produced by the circuit that replaces the encoder by three Hadamard gates, as shown in Figure 12. After applying the Hadamard gates below the unknown input state $|\psi\rangle = \alpha|0\rangle + \beta|1\rangle$, the system is found

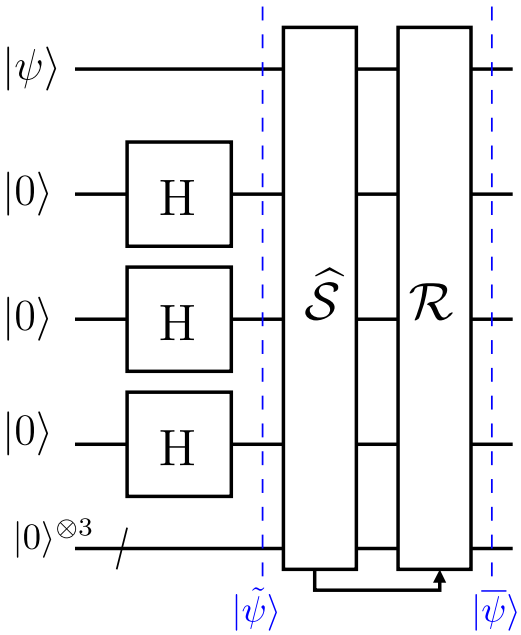

FIGURE 12. Encoderless Steane Code with three Hadamard Gates.

in the state

$$\begin{aligned}|\tilde{\psi}\rangle = (\alpha|0\rangle + \beta|1\rangle) &\otimes \left(\frac{|0\rangle + |1\rangle}{\sqrt{2}}\right) \\ &\otimes \left(\frac{|0\rangle + |1\rangle}{\sqrt{2}}\right) \otimes \left(\frac{|0\rangle + |1\rangle}{\sqrt{2}}\right) \otimes |000\rangle.\end{aligned} \tag{37}$$

Expanding this gives

$$\begin{aligned}|\tilde{\psi}\rangle = \frac{\alpha}{\sqrt{8}}&[\underline{|0000000\rangle} + |0010000\rangle + |01000000\rangle \\ &+ |0110000\rangle + |0001000\rangle + |0011000\rangle \\ &+ |0101000\rangle + |0111000\rangle] \\ &+ \frac{\beta}{\sqrt{8}}[\underline{|1110000\rangle} + |1000000\rangle + |1010000\rangle \\ &+ |1100000\rangle + |1001000\rangle + |1011000\rangle \\ &+ |1101000\rangle + |1111000\rangle].\end{aligned} \tag{38}$$

The underlined vectors represent those that overlap with the conventionally encoded state shown in Eq. (36). The vectors that are not underlined represent errors that can be corrected. Then by the same reasoning as for the repetition code of Section II-A, the encoded state in Eq. (36) is fixed after the application of the stabilizer operators in Eq. (4).

Then the vectors that are not underlined are corrected by the syndrome decoder of Figure 13. This is shown by Eq. (17). We can readily see that the encoded state in Eq (36) can be recovered by the following calculations

$$\begin{aligned}|\psi_1\rangle &= \frac{1}{2}(|\tilde{\psi}\rangle + K_1|\tilde{\psi}\rangle) \\ |\psi_2\rangle &= \frac{1}{2}(|\psi_1\rangle + K_2|\psi_1\rangle) \\ |\psi_3\rangle &= \frac{1}{2}(|\psi_2\rangle + K_3|\psi_2\rangle) \\ |\psi_4\rangle &= \frac{1}{2}(|\psi_3\rangle + K_4|\psi_3\rangle)\end{aligned}$$

$$|\psi_5\rangle = \frac{1}{2}(|\psi_4\rangle + K_5|\psi_4\rangle)$$
$$|\psi_6\rangle = \frac{1}{2}(|\psi_5\rangle + K_6|\psi_5\rangle) = |\overline{\psi}\rangle, \quad (39)$$

where K_1 to K_6 corresponds to the Steane code stabilizers in Eq. (4). Therefore the encoderless schemes can be readily combined with transversal gates in the same way, as described for the repetition code of Section II-B. The full scheme is shown in Figure 13.

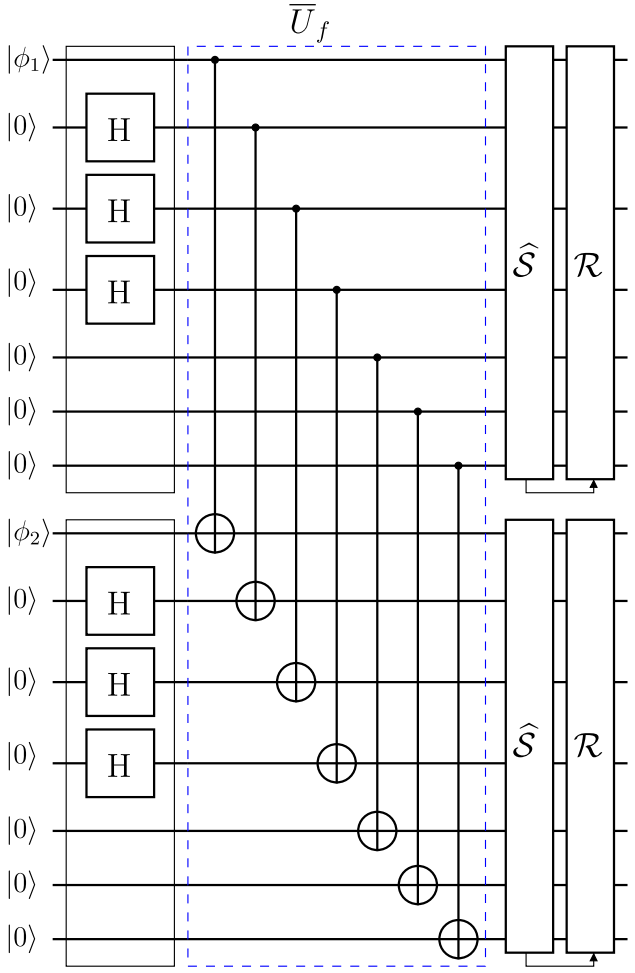

FIGURE 13. Full Scheme of the Transversal CNOT gate with the encoderless Steane code.

B. FURTHER IMPROVEMENTS

The number of Hadamard gates in the scheme seen in Figure 13 can be reduced to as few as two, which is shown in Figure 14. Let us elaborate on this scenario by using the same method as that in the previous section. If we have $|\phi_1\rangle = \alpha|0\rangle + \beta|1\rangle$, the top encoded qubit of Figure 14 can be described by

$$|\tilde{\psi}\rangle = |0\rangle \otimes (\alpha|0\rangle + \beta|1\rangle) \otimes |0\rangle \otimes \left(\frac{|0\rangle + |1\rangle}{\sqrt{2}}\right) \otimes |0\rangle \otimes \left(\frac{|0\rangle + |1\rangle}{\sqrt{2}}\right) \otimes |0\rangle. \quad (40)$$

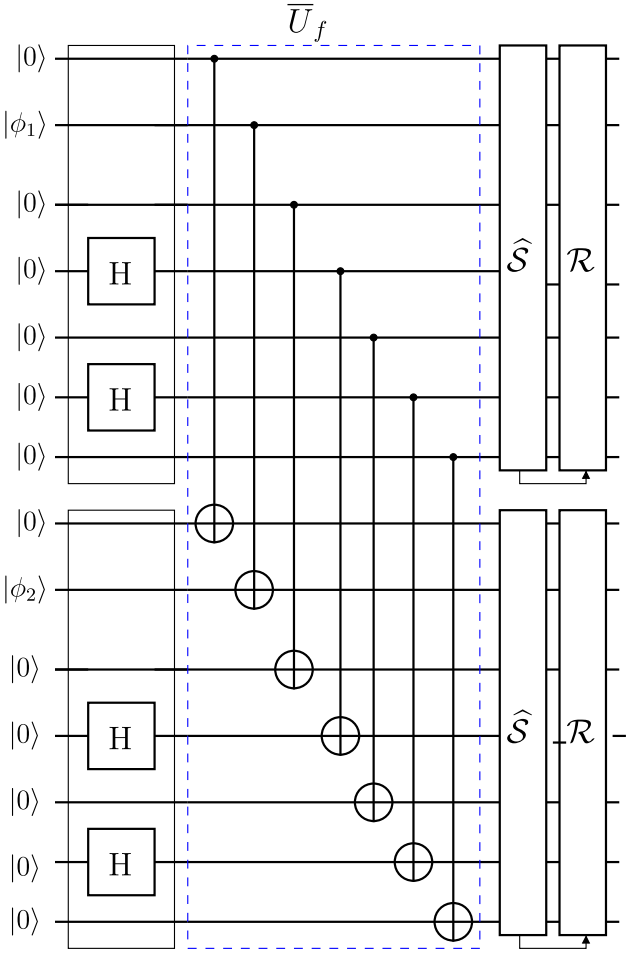

FIGURE 14. Encoderless Steane Code with two Hadamard Gates.

This may be expanded to give

$$|\tilde{\psi}\rangle = \frac{\alpha}{\sqrt{8}}[\underline{|0000000\rangle} + |0000010\rangle + |0001000\rangle + |0001010\rangle] + \frac{\beta}{\sqrt{8}}[\underline{|0101010\rangle} + |0101000\rangle + |0100010\rangle + |0100000\rangle], \quad (41)$$

where the underlined vectors overlap with the conventionally encoded state in Eq. (36). After the application of the syndrome decoder, the encoded state in Eq. (36) can be recovered as shown in Eq. (39).

This methodology can also be applied to other codes, where the positioning of Hadamard gates and of the original information qubit $|\phi_1\rangle = \alpha|0\rangle + \beta|1\rangle$ are arragned for ensuring that a single vector belonging to the logical state $|\overline{0}\rangle$ appears with an $\frac{\alpha}{\sqrt{2}}$ coefficient. Likewise, a single vector belonging to the logical $|\overline{1}\rangle$ state appears with an $\frac{\beta}{\sqrt{2}}$ coefficient. Therefore, where the code satisfies the property that $|\overline{1}\rangle = X^{\otimes 7}|\overline{0}\rangle$ the vectors with the smallest (classical) weight indicate the position of the smallest number of Hadamard gates. Then the application of the stabilizer measurements

projects this expansion to the correctly encoded state $\overline{\psi}\rangle = \alpha|\overline{0}\rangle + \beta|\overline{1}\rangle$. Therefore it is feasible that the broad class of QSCs may exhibit encoderless properties, provided that stabilizer measurements can be implemented fault-tolerantly.

C. SIMULATION RESULTS & DISCUSSIONS

Figure 15 shows that the FER upper bound of the encoderless scheme is $FER = 78P_g^2$ which is derived by the probability of two simultaneous gate errors of Figure 13 by

$$FER \leq \sum_{i=1}^{\mathcal{D}} \eta_i P_g^i \quad \text{where} \quad \eta_i = \binom{\mathcal{D}}{i}. \tag{42}$$

Observe in Figure 15 that the simulation results appear to be better than the estimated 'upper bound' indicating that there are certain simultaneous two-gate errors that actually impose qubit error that can be corrected by the syndrome decoder. The gate error rate below which the scheme offers an CNOT gate accuracy better than an uncoded gate is seen to be $P_{th} = 0.024$.Naturally we aim for $P_g < P_{th}$. Furthermore, to achieve a FER less than 10^{-4} this scheme requires individual components having a gate error probability lower than 10^{-3}, as seen in Figure 15.

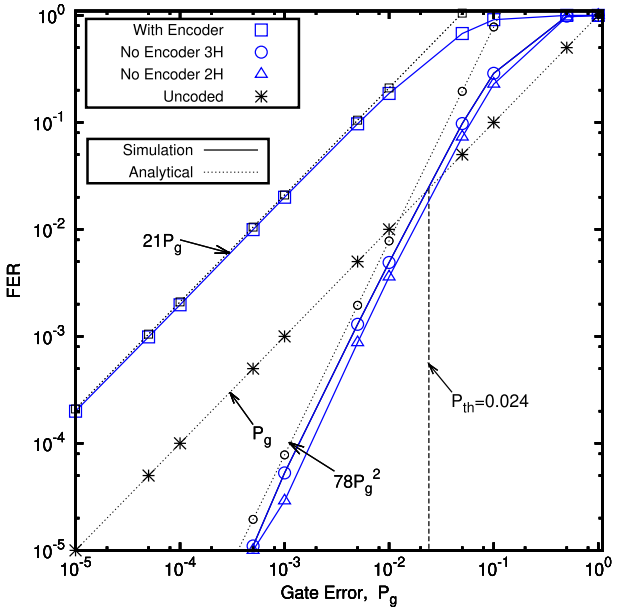

FIGURE 15. Encoderless scheme comparing the systems of Figure 13 (3H) and Figure 14 (2H). The analytical circle represents the upper bound and the square is a tighter bound.

The encoderless scheme provides better-than-uncoded FER performance for both the bit-flip and depolarizing channel. This is because the scheme dispenses with the non-fault-tolerant traditional encoding circuits, which increase the qubit error probability owing to error proliferation. Therefore the encoderless scheme of Figure 14 provides a compelling proof-of-concept for implementing QECCs fault-tolerantly without any initial assumption about the information being computed. Moreover the encoderless scheme provides a FER improvement for Steane's code even when constructed from imperfect gates.

QECCs constructed based on traditional encoding circuits have the advantage that they are capable of encoding unknown information. However these circuits are not fault-tolerant [1]. Hence techniques of encoding known information without a traditional encoding circuit have been investigated in [35] for example. However these schemes have the drawback that only certain simple quantum states can be encoded. By contrasting the scheme presented here circumvents these issues by using stabilizer measurements for encoding unknown states. This means that an additional error correction step is required, which has a substantial qubit overhead, when implemented fault-tolerantly, as described in Section I-C. Nevertheless, these results provide a proof-of-concept for the family of the techniques that are capable of encoding any arbitrary information without the need for non-fault-tolerant encoding circuits.

IV. STATE PREPARATION

This section investigates how the known state $|\psi\rangle = |0\rangle$ can be encoded by applying certain Steane code stabilizers to a specific input state [35]. This circumvents the application of the traditional unitary encoding circuit characterised by Eq. (1) albeit with the drawback that the state that is being encoded must be known [1]. The basic idea is that the stabilizers K_1, K_2 and K_3 in Eq. (4) are applied to the all-zero qubit input state $|\tilde{\psi}\rangle = |0\rangle^{\otimes 7}$, as shown in Figure 16. This gives $|\overline{\psi}\rangle = |\overline{0}\rangle$ in Eq. (2), which is the encoded version of $|\psi\rangle = |0\rangle$. It is not necessary to apply the full stabilizer set, because $|\tilde{\psi}\rangle = |0\rangle^{\otimes n}$ is already a $+1$ eigenvalue of K_1, K_2 and K_3 [32].

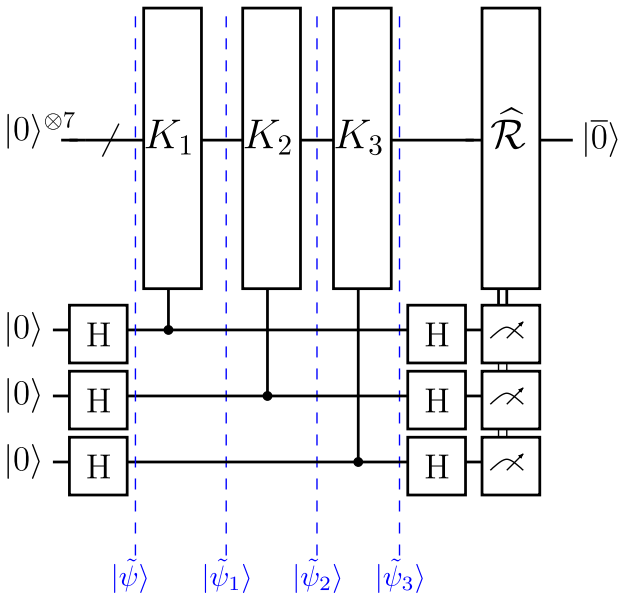

FIGURE 16. Preparing the known state $|\overline{0}\rangle$ encoded by the Steane code using the stabilizer measurements of K_1, K_2 and K_3 in Eq. (4).

Let us consider the most straightforward scenario, whereby the measurement of the stabilizers K_1, K_2 and K_3 in Eq. (4) results in the $|0\rangle$ state in the ancilla, as described by Eq. (18). If the measurement of $K_1 = IIIXXXX$ results in $|0\rangle$ in the ancilla, the system is in the state of

$$|\tilde{\psi}_1\rangle = \frac{1}{2}\big(|\tilde{\psi}\rangle + K_1|\tilde{\psi}\rangle\big) = |0000000\rangle + |0001111\rangle. \quad (43)$$

This state is input to the $K_2 = XIXIXIX$ stabilizer, which is also measured in the $|0\rangle$ state. Then $|\tilde{\psi}_2\rangle$ describes the system after this measurement

$$|\tilde{\psi}_2\rangle = \frac{1}{2}\big(|\tilde{\psi}_1\rangle + K_2|\tilde{\psi}_1\rangle\big) = |0000000\rangle + |0001111\rangle + \quad (44)$$

$$|1010101\rangle + |1011010\rangle. \quad (45)$$

Finally the $|0\rangle$ state is measured in the ancilla, when the $K_3 = IXXIIXX$ stabilizer is applied to the state in $|\tilde{\psi}_2\rangle$. This gives

$$\begin{aligned}|\tilde{\psi}_3\rangle = \frac{1}{2}\big(|\tilde{\psi}_2\rangle + K_3|\tilde{\psi}_2\rangle\big) &= |0000000\rangle + |0001111\rangle \\ &+ |1010101\rangle + |1011010\rangle + |0110011\rangle \\ &+ |0111100\rangle + |1100110\rangle + |1101001\rangle \\ &= |\overline{0}\rangle, \end{aligned} \quad (46)$$

which is the Steane encoded $|\overline{\psi}\rangle = |\overline{0}\rangle$ in Eq. (2).

Once the encoded $|\overline{0}\rangle$ state is prepared, it becomes possible to prepare the encoded version of any arbitrary state $|\psi\rangle = \alpha|0\rangle + \beta|1\rangle$, provided that we know the value of α and β [2]. This is possible as long as the processor has an encoded universal gate set as defined in [36]. This will mean that any arbitrary gate operation can be applied to the encoded data allowing the encoded zero state to be transformed to any arbitrary superposition of code word basis states. For example, we might like to prepare the encoded sate $|\overline{\psi}\rangle = |\overline{1}\rangle$, where $\beta = 1$. This can be done by preparing the $|\overline{0}\rangle$ state as outlined above and then applying the transversal bit-flip gate as follows

$$\overline{X}|\overline{0}\rangle \rightarrow |\overline{1}\rangle, \quad (47)$$

therefore preparing $|\overline{\psi}\rangle = |\overline{1}\rangle$. Similarly, to prepare the encoded version of the equi-probable superposition state of

$$|\overline{\psi}\rangle = \frac{|\overline{0}\rangle + |\overline{1}\rangle}{\sqrt{2}}, \quad (48)$$

the same method may be employed. First the encoded $|\overline{0}\rangle$ state in Eq. (2) is prepared, followed by the application of the transversal Hadamard gate,

$$\overline{H}|\overline{0}\rangle \rightarrow \frac{|\overline{0}\rangle + |\overline{1}\rangle}{\sqrt{2}}. \quad (49)$$

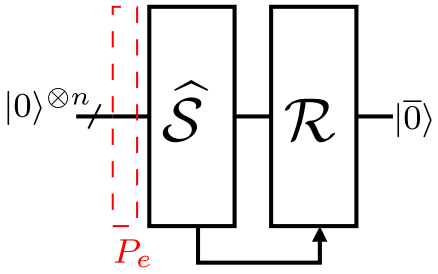

FIGURE 17. Preparing the Steane encoded $|\overline{0}\rangle$ state.

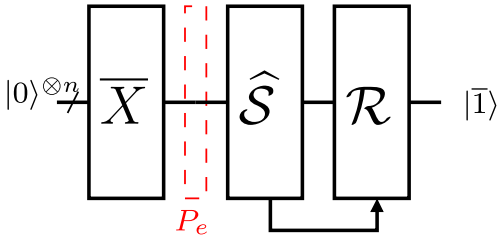

FIGURE 18. Preparing the Steane encoded $|\overline{1}\rangle$ state.

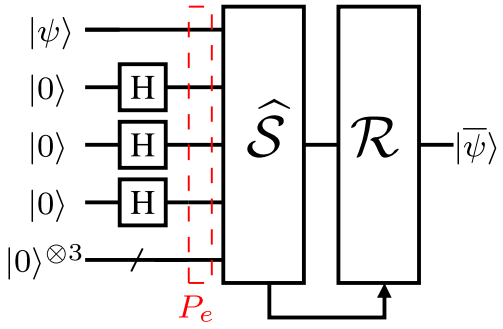

FIGURE 19. Preparing the unknown Steane encoded $|\overline{\psi}\rangle$ state without an encoder using 3 Hadamard gates.

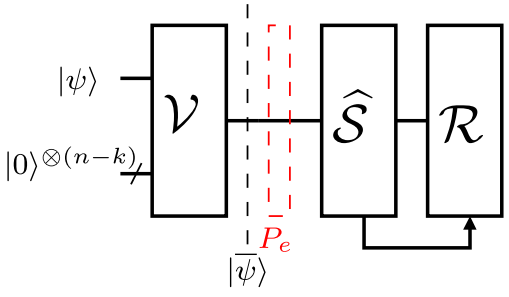

FIGURE 20. Preparing the unknown Steane encoded $|\overline{\psi}\rangle$ state with traditional Steane encoder.

A. SYSTEM MODEL

In this system the encoded version of various single qubit states is encoded by the Steane code, therefore in general this system has the transformation $|\psi\rangle \rightarrow |\overline{\psi}\rangle$. This is seen in 19, 20 and Figure 21, where any unknown state is

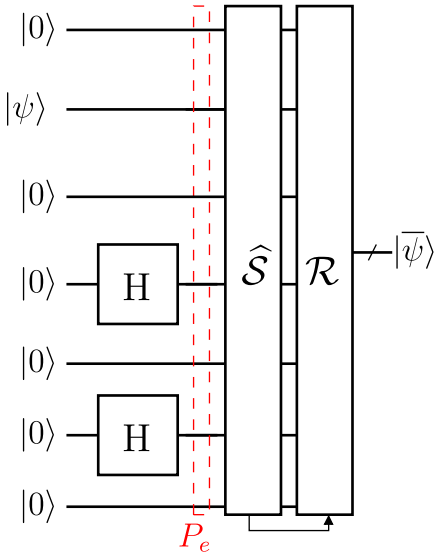

FIGURE 21. Preparing the unknown Steane encoded $|\overline{\psi}\rangle$ state without encoder using two Hadamard gates.

prepared. The known state preparation constituted a specific case of these schemes, as seen in Figure 17, 18 and 22. For example in Figure 17 we can see that $|0\rangle \rightarrow |\overline{0}\rangle$. The encoded $|\overline{1}\rangle$ described in Eq. (47) is shown in Figure 18. Moreover, the encoded $|\overline{+}\rangle$ described in Eq. (49) is shown in Figure 22. Each scheme is simulated in the face of gate errors as well as qubit decoherence error probability of P_e before the syndrome decoder in Figure 17, 18 and 22. Therefore Figure 22 has an additional syndrome decoder, meaning that the $|0\rangle$ state is prepared to achieve the transformation seen in Eq. (49). There may be circuit implementations that have a reduced number of syndrome decoding steps, reminiscent of the approach taken in Section II-B. However, this is not explored here. Since a single qubit state is encoded (not a quantum gate) the uncoded scheme has an error rate of $FER = P_e$.

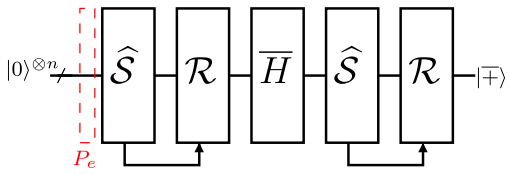

FIGURE 22. Preparing the Steane encoded $|\overline{+}\rangle$ state.

B. RESULTS AND DISCUSSION

In this simulation we assume that both the stabilizer and the error recovery circuits of Figure 17, 18 and 22 are fault-tolerant (see SectionI-C) and incur a negligible error rate. Therefore the FER associated with preparing the encoded $|\overline{0}\rangle$ state is upper bounded by $\binom{7}{2}P_e^2$. The scheme shown in Figure 21 demonstrates the best FER performance of encoding an unknown input state. See Table 4 for

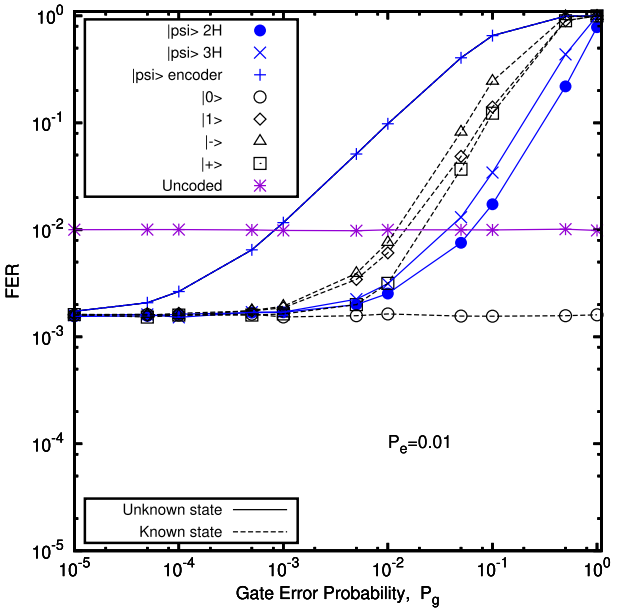

FIGURE 23. FER vs. P_g for State Preparation aided Steane encoded states at $P_e = 10^{-2}$.

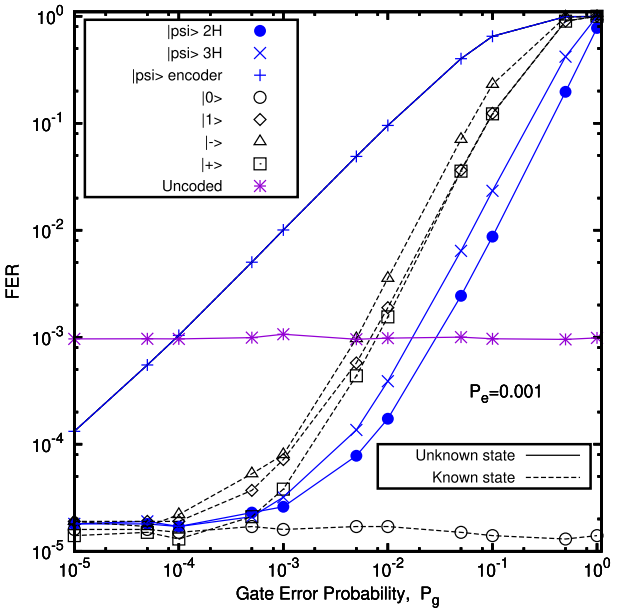

FIGURE 24. FER vs. P_g for State Preparation aided Steane encoded states at $P_e = 10^{-3}$.

TABLE 4. Table summarising the results in Figure 23-28 for the 2H encoderless scheme.

Summary of Fig. 23-28			
Fig.	P_g	P_e	$FER \approx$
23-24	5×10^{-3}	10^3	10^4
25-26	10^2	10^4	10^4
27-28	10^3	5×10^4	10^5

a summary of results of this scheme in Figures 23-28. This is due to the low complexity of its circuit, which helps in

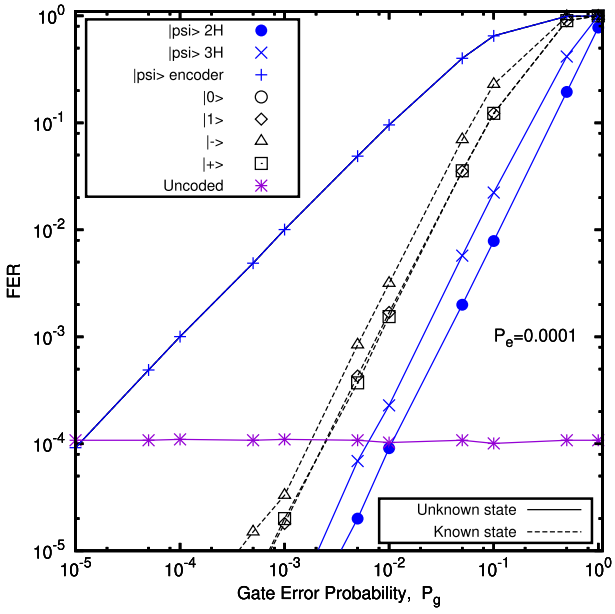

FIGURE 25. FER vs. P_g for State Preparation aided Steane encoded states at $P_e = 10^{-4}$.

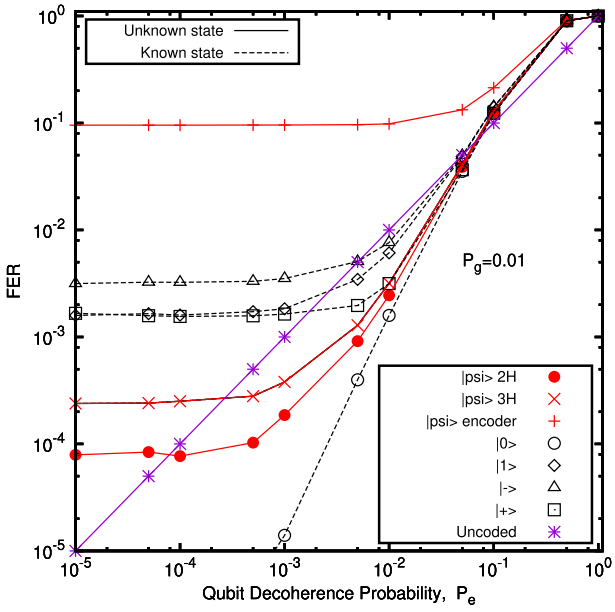

FIGURE 26. FER vs. P_e for State Preparation aided Steane encoded states at $P_g = 10^{-2}$.

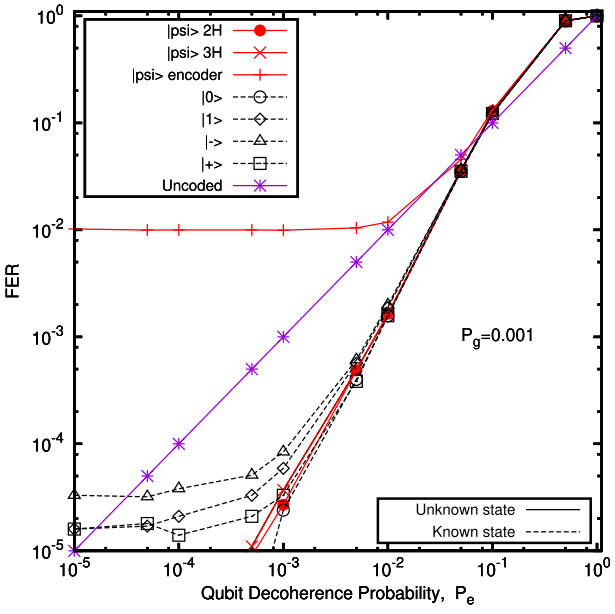

FIGURE 27. FER vs. P_e for State Preparation aided Steane encoded states at $P_g = 10^{-3}$.

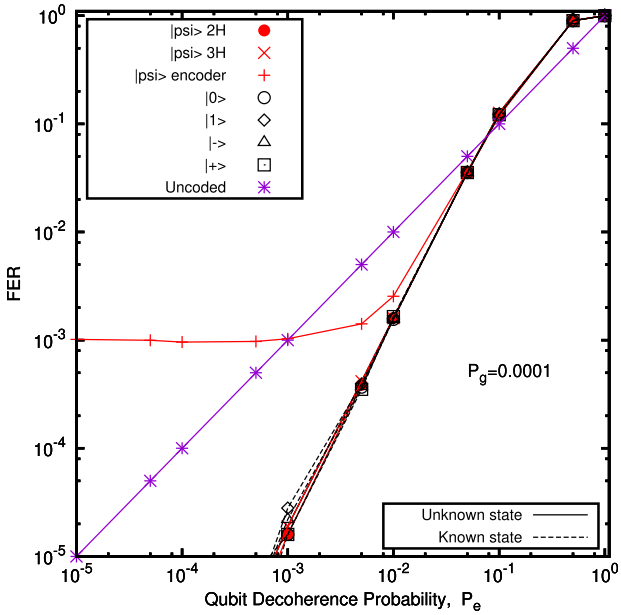

FIGURE 28. FER vs. P_e for State Preparation aided Steane encoded states at $P_g = 10^{-4}$.

limiting the error proliferation. For example, when $P_e = 0.01$ (Figure 23) and $P_g = 0.005$ the scheme relying on a traditional encoding circuit has a FER 386% higher than the encoderless scheme using two Hadamard gates. To achieve $FER \approx 10^{-5}$, a gate error probability of $P_g = 5 \times 10^{-5}$ and $P_e = 10^{-3}$ are required, as shown in Figure 24. In this case the encoderless 2H scheme achieves a FER almost two orders of magnitude lower than that of the uncoded scheme. Where gate error probability is $P_g > 10^{-3}$, $FER < 10^{-4}$ can be achieved, provided that the qubit decoherence is below ($P_e = 10^{-4}$), as seen in Figure 25.

When the gate error probability is as high as $P_g = 0.01$, the encoderless scheme achieves only a modest improvement on the uncoded scheme, namely a 24% reduction in FER at $P_e = 10^{-4}$, as seen in Figure 26. However, Figure 27

shows that when the gate error probability is $P_g = 10^{-3}$, then a qubit decoherence at $P_e = 5 \times 10^{-4}$ can be tolerated, while still achieving $FER < 10^{-5}$. In this case the 'Three Hadamard Gate Encoderless scheme' reduces the error rate by three orders of magnitude compared to the scheme using the traditional encoder. This is because the circuit in Figure 1 is not fault-tolerant and therefore the gate error probabiltiy dominates the FER. For even further improvements a smaller gate error is required, as seen in Figure 28, where $P_g = 10^{-4}$.

V. CONCLUSION

The encoderless scheme achieves better FER performance since the complexity of the circuit it reduced. The arrangement of fewer single qubit gates means that the circuit is fault-tolerant leading to a FER crossover with the uncoded scheme, where $P_g < P_{th}$. This can be applied to state preparation where the encoderless quantum codes outperform the preparation of $|\overline{1}\rangle$, $|\overline{+}\rangle$ and $|\overline{-}\rangle$ states. However the simplicity of the preparation of the $|\overline{0}\rangle$ state means that this achieves the best FER performance. These schemes offer significant improvements on the traditional encoder which cannot offer a FER better than the uncoded scheme.

The unknown state may be replaced by a known state for and the encoderless scheme may offer a better scheme. This is a promising avenue for future research. In addition the stabilizer set may be reduced for certain cases, and additional insight can be obtained by simulating error propagation in these circuits.

REFERENCES

[1] J. Preskill, "Fault-tolerant quantum computation," in *Introduction to Quantum Computation and Information*. Singapore: World Scientific, 1998, pp. 213–269.

[2] M. A. Nielsen and I. Chuang, *Quantum Computation and Quantum Information*. Cambridge, U.K.: Cambridge Univ. Press, 2010.

[3] R. Cane, D. Chandra, S. X. Ng, and L. Hanzo, "Mitigation of decoherence-induced quantum-bit errors and quantum-gate errors using Steane's code," *IEEE Access*, vol. 8, pp. 83693–83709, 2020.

[4] D. Gottesman, "Theory of fault-tolerant quantum computation," *Phys. Rev. A, Gen. Phys.*, vol. 57, no. 1, p. 127, 1998.

[5] P. W. Shor, "Fault-tolerant quantum computation," in *Proc. 37th Conf. Found. Comput. Sci.*, Oct. 1996, pp. 56–65.

[6] A. M. Steane, "Fast fault-tolerant filtering of quantum codewords," 2002, *arXiv:quant-ph/0202036*. [Online]. Available: https://arxiv.org/abs/quant-ph/0202036

[7] C.-Y. Lai, Y.-C. Zheng, and T. A. Brun, "Fault-tolerant preparation of stabilizer states for quantum Calderbank-Shor-Steane codes by classical error-correcting codes," *Phys. Rev. A, Gen. Phys.*, vol. 95, no. 3, Mar. 2017, Art. no. 032339.

[8] P. Aliferis, D. Gottesman, and J. Preskill, "Quantum accuracy threshold for concatenated distance-3 codes," 2005, *arXiv:quant-ph/0504218*. [Online]. Available: https://arxiv.org/abs/quant-ph/0504218

[9] E. Knill, "Quantum computing with realistically noisy devices," *Nature*, vol. 434, no. 7029, pp. 39–44, 2005.

[10] H. Goto, "Minimizing resource overheads for fault-tolerant preparation of encoded states of the Steane code," *Sci. Rep.*, vol. 6, no. 1, p. 19578, Apr. 2016.

[11] A. Paetznick and B. W. Reichardt, "Fault-tolerant ancilla preparation and noise threshold lower bounds for the 23-qubit golay code," 2011, *arXiv:1106.2190*. [Online]. Available: http://arxiv.org/abs/1106.2190

[12] K. M. Svore, D. P. DiVincenzo, and B. M. Terhal, "Noise threshold for a fault-tolerant two-dimensional lattice architecture," 2006, *arXiv:quant-ph/0604090*. [Online]. Available: https://arxiv.org/abs/quant-ph/0604090

[13] F. M. Spedalieri and V. P. Roychowdhury, "Latency in local, two-dimensional, fault-tolerant quantum computing," 2008, *arXiv:0805.4213*. [Online]. Available: http://arxiv.org/abs/0805.4213

[14] J. Preskill, "Quantum computing in the NISQ era and beyond," 2018, *arXiv:1801.00862*. [Online]. Available: http://arxiv.org/abs/1801.00862

[15] D. Chandra, Z. Babar, H. V. Nguyen, D. Alanis, P. Botsinis, S. X. Ng, and L. Hanzo, "Quantum topological error correction codes are capable of improving the performance of clifford gates," *IEEE Access*, vol. 7, pp. 121501–121529, 2019.

[16] A. M. Steane, "Active stabilization, quantum computation, and quantum state synthesis," *Phys. Rev. Lett.*, vol. 78, no. 11, p. 2252, 1997.

[17] P. W. Shor, "Scheme for reducing decoherence in quantum computer memory," *Phys. Rev. A, Gen. Phys.*, vol. 52, no. 4, pp. R2493–R2496, Oct. 1995.

[18] A. R. Calderbank and P. W. Shor, "Good quantum error-correcting codes exist," *Phys. Rev. A, Gen. Phys.*, vol. 54, no. 2, p. 1098, 1996.

[19] A. M. Steane, "Error correcting codes in quantum theory," *Phys. Rev. Lett.*, vol. 77, no. 5, p. 793, 1996.

[20] C. H. Bennett, D. P. DiVincenzo, J. A. Smolin, and W. K. Wootters, "Mixed-state entanglement and quantum error correction," *Phys. Rev. A, Gen. Phys.*, vol. 54, no. 5, p. 3824, Nov. 1996.

[21] R. Laflamme, C. Miquel, J. P. Paz, and W. H. Zurek, "Perfect quantum error correcting code," *Phys. Rev. Lett.*, vol. 77, no. 1, p. 198, 1996.

[22] D. Gottesman, "Stabilizer codes and quantum error correction," 1997, *arXiv:quant-ph/9705052*. [Online]. Available: https://arxiv.org/abs/quant-ph/9705052

[23] D. Gottesman, "Class of quantum error-correcting codes saturating the quantum Hamming bound," *Phys. Rev. A, Gen. Phys.*, vol. 54, no. 3, p. 1862, 1996.

[24] Z. Babar, P. Botsinis, D. Alanis, S. Xin Ng, and L. Hanzo, "The road from classical to quantum codes: A hashing bound approaching design procedure," *IEEE Access*, vol. 3, pp. 146–176, 2015.

[25] D. Chandra, Z. Babar, H. V. Nguyen, D. Alanis, P. Botsinis, S. X. Ng, and L. Hanzo, "Quantum coding bounds and a closed-form approximation of the minimum distance versus quantum coding rate," *IEEE Access*, vol. 5, pp. 11557–11581, 2017.

[26] A. Y. Kitaev, "Quantum error correction with imperfect gates," in *Quantum Communication, Computing, and Measurement*. New York, NY, USA: Springer, 1997, pp. 181–188.

[27] D. P. DiVincenzo and P. W. Shor, "Fault-tolerant error correction with efficient quantum codes," *Phys. Rev. Lett.*, vol. 77, no. 15, p. 3260, 1996.

[28] R. Chao and B. W. Reichardt, "Quantum error correction with only two extra qubits," *Phys. Rev. Lett.*, vol. 121, no. 5, Aug. 2018, Art. no. 050502.

[29] B. W. Reichardt, "Improved ancilla preparation scheme increases fault-tolerant threshold," 2004, *arXiv:quant-ph/0406025*. [Online]. Available: https://arxiv.org/abs/quant-ph/0406025

[30] D. Gottesman, "An introduction to quantum error correction and fault-tolerant quantum computation," in *Quantum Information Science and Its Contributions to Mathematics, Proceedings of Symposia in Applied Mathematics*, vol. 68. Washington, DC, USA: American Mathematical Society, 2010, pp. 13–58.

[31] C. Zalka, "Threshold estimate for fault tolerant quantum computation," 1996, *arXiv:quant-ph/9612028*. [Online]. Available: https://arxiv.org/abs/quant-ph/9612028

[32] S. J. Devitt, W. J. Munro, and K. Nemoto, "Quantum error correction for beginners," *Rep. Prog. Phys.*, vol. 76, no. 7, 2013, Art. no. 076001.

[33] E. T. Campbell, B. M. Terhal, and C. Vuillot, "Roads towards fault-tolerant universal quantum computation," *Nature*, vol. 549, no. 7671, pp. 172–179, 2017.

[34] Z. Babar, D. Chandra, H. V. Nguyen, P. Botsinis, D. Alanis, S. X. Ng, and L. Hanzo, "Duality of quantum and classical error correction codes: Design principles and examples," *IEEE Commun. Surveys Tuts.*, vol. 21, no. 1, pp. 970–1010, 1st Quart., 2019.

[35] E. Knill, "Fault-tolerant postselected quantum computation: Schemes," 2004, *arXiv:quant-ph/0402171*. [Online]. Available: https://arxiv.org/abs/quant-ph/0402171

[36] A. Y. Kitaev, "Quantum computations: Algorithms and error correction," *Russian Math. Surv.*, vol. 52, no. 6, pp. 1191–1249, Dec. 1997.

ROSIE CANE received the B.Sc. degree (Hons.) in physics and maths from The Open University, U.K., in 2015, and the M.Sc. degree in wireless communications from the University of Southampton, in 2017, where she is currently pursuing the Ph.D. degree with the Next Generation Wireless Research Group, School of Electronics and Computer Science. Her research interests include quantum computation and quantum information theory, quantum communications, and quantum error correction codes.

DARYUS CHANDRA received the M.Eng. degree in electrical engineering from Universitas Gadjah Mada, Indonesia, in 2014, and the Ph.D. degree with the Next Generation Wireless Research Group, School of Electronics and Computer Science, University of Southampton, U.K., in 2019. He is currently a Postdoctoral Research Fellow with the Department of Electrical Engineering and Information Technology, University of Naples Federico II, Italy. His research interests include classical and quantum error correction codes, quantum information, and quantum communications. He was a recipient of the Scholarship Award from the Indonesia Endowment Fund for Education (Lembaga Pengelola Dana Pendidikan).

SOON XIN NG (Senior Member, IEEE) received the B.Eng. degree (Hons.) in electronic engineering and the Ph.D. degree in telecommunications from the University of Southampton, Southampton, U.K., in 1999 and 2002, respectively. From 2003 to 2006, he was a Postdoctoral Research Fellow working on collaborative European research projects known as SCOUT, NEWCOM, and PHOENIX. Since August 2006, he has been a Member of Academic Staff with the School of Electronics and Computer Science, University of Southampton. He is currently an Associate Professor of telecommunications with the University of Southampton. He is involved in the OPTIMIX and CONCERTO European projects as well as the IU-ATC and UC4G projects. His research interests include adaptive coded modulation, coded modulation, channel coding, space-time coding, joint source and channel coding, iterative detection, OFDM, MIMO, cooperative communications, distributed coding, quantum error correction codes, and joint wireless-and-optical-fibre communications. He has published over 200 articles and co-authored two John Wiley/IEEE Press books in this field. He is also a Chartered Engineer and a Fellow of the Higher Education Academy in the U.K.

LAJOS HANZO (Fellow, IEEE) received the master's and Ph.D. degrees from the Technical University (TU) of Budapest, in 1976 and 1983, respectively. He has served several terms as the Governor of both IEEE ComSoc and of VTS. He has published more than 1900 contributions at the IEEE Xplore and 19 Wiley-IEEE Press books. He has helped the fast-track career of 123 Ph.D. students. Over 40 of them are Professors at various stages of their careers in academia and many of them are leading scientists in the wireless industry. He is also a Fellow of the Royal Academy of Engineering (REng), IET, and EURASIP. He was awarded the Doctor of Sciences (D.Sc.) degree by the University of Southampton in 2004, and the Honorary Doctorates by the TU of Budapest in 2009 and by The University of Edinburgh in 2015. He is also a Foreign Member of the Hungarian Academy of Sciences and a former Editor-in-Chief of the IEEE Press.